AD-A179 408 HIGH-STRAIN-RATE BEHAVIOR OF HYDRATED CEMEN PASTE(U) 1/1
MARTIN MARIETTA LABS BALTIMORE MD I JAWED ET AL.
29 JAN 87 MML-TR-87-12C AFOSR-TR-87-0444
UNCLASSIFIED F49620-86-C-0021 F/G 11/2 NL

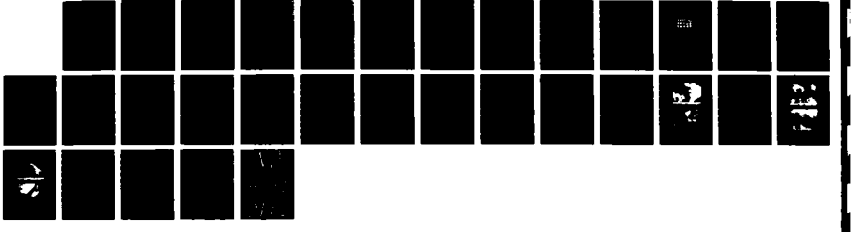

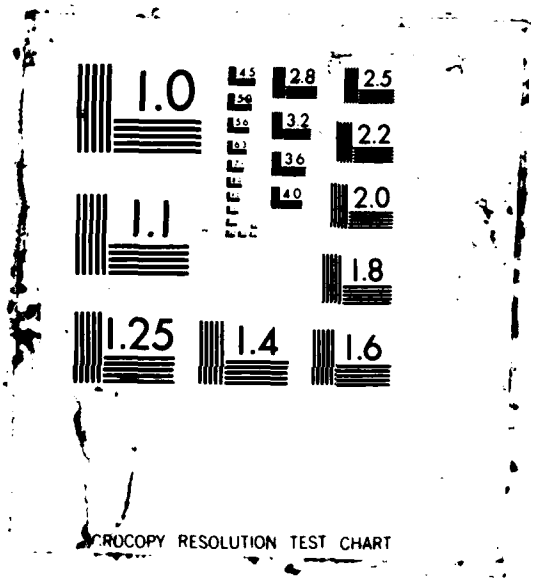
1.0
1.1
1.25
1.4
1.6
2.8
3.2
3.6
4.0
2.5
2.2
2.0
1.8
CROCOPY RESOLUTION TEST CHART

AFOSR-TR- 87-0144

MARTIN MARIETTA

SECURITY CLASSIFICATION OF THIS PAGE (When Data Entered)

REPORT DOCUMENTATION PAGE

READ INSTRUCTIONS BEFORE COMPLETING FORM

1. REPORT NUMBER: AFOSR-TR- 87-0444
2. GOVT ACCESSION NO.
3. RECIPIENT'S CATALOG NUMBER

4. TITLE (and Subtitle): High-Strain-Rate Behavior of Hydrated Cement Paste
5. TYPE OF REPORT & PERIOD COVERED: Technical Report Jan. 1, 1986 - Jan. 29, 1987
6. PERFORMING ORG. REPORT NUMBER: MML TR 87-12c

7. AUTHOR(s): I. Jawed, G. Childs, A. Ritter, S. Winzer D.B. Barker, and T. Johnson

8. CONTRACT OR GRANT NUMBER(s): F49620-86-C-0021

9. PERFORMING ORGANIZATION NAME AND ADDRESS: Martin Marietta Laboratories 1450 South Rolling Road Baltimore, Maryland 21227

10. PROGRAM ELEMENT, PROJECT, TASK AREA & WORK UNIT NUMBERS: 61102F 2302/C2

11. CONTROLLING OFFICE NAME AND ADDRESS: Air Force Office of Scientific Research Bolling Air Force Base Washington, DC 20332-6448 NA

12. REPORT DATE: Jan. 29, 1987

13. NUMBER OF PAGES: 25

14. MONITORING AGENCY NAME & ADDRESS (if different from Controlling Office): Same as 11

15. SECURITY CLASS. (of this report): Unclassified

15a. DECLASSIFICATION DOWNGRADING SCHEDULE

16. DISTRIBUTION STATEMENT (of this Report)

"A"

Approved for public release; distribution unlimited.

17. DISTRIBUTION STATEMENT (of the abstract entered in Block 20, if different from Report)

18. SUPPLEMENTARY NOTES

19. KEY WORDS (Continue on reverse side if necessary and identify by block number)

Cement paste, strain rate, ultimate stress, microstructure.

20. ABSTRACT (Continue on reverse side if necessary and identify by block number)

Two distinct trends in the stress-strain behavior of cement pastes hydrated for 28 days were noted. At low strain rates (<250/sec) the ultimate stress increases almost linearly, whereas at higher rate (> 250/sec) it reaches a somewhat limiting value. Porosity of the pastes appears to be the dominant factor in determining the strain-rate response. Fractures and cracks under loading are seen to go through the C-S-H phase of the paste.

DD FORM 1 JAN 73 1473 EDITION OF 1 NOV 65 IS OBSOLETE

SECURITY CLASSIFICATION OF THIS PAGE (When Data Entered)

MML TR 87-12c

HIGH-STRAIN-RATE BEHAVIOR OF HYDRATED CEMENT PASTE

ANNUAL REPORT

Period: January 1, 1986 - January 29, 1987

Contract No.: F49620-86-C-0021

Submitted to:

Air Force Office of Scientific Research
Bolling Air Force Base
Washington, DC 20332-6448

Submitted by:

I. Jawed, G. Childs, A. Ritter and S. Winzer

Martin Marietta Laboratories
1450 South Rolling Road
Baltimore, Maryland 21227-3898

and

D.B. Barker and T. Johnson

University of Maryland
College Park, Maryland 20742

January 1987

TABLE OF CONTENTS

LIST OF TABLES

LIST OF FIGURES

I. INTRODUCTION

The use of concrete as a basic structural material makes it increasingly important to improve both our understanding of its behavior, and our ability to accurately predict its response under load. While the behavior of concrete under static and quasi-dynamic loadings appears to be reasonably well understood, the same cannot be said about its behavior under dynamic tensile and compressive loadings. Predicting the structural response under such loading rates, and accounting for it, is of critical importance in the design of civilian structures, such as fallout shelters and nuclear containment structures, and military construction, such as bunkers and ammunition depots.

Recently, there has been increasing interest in the effects of high strain rates on the mechanical properties of concrete and other cementitious materials.[1] However, little is known in this area because there is little information on the effect of high strain rates and high peak loads on the microstructure of concrete. Gaining this knowledge is a difficult task because of the extreme complexity of the microstructure of concrete -- a composite material consisting of several hydrated and unhydrated cement minerals, fine and coarse aggregates, chemical admixtures, and water. Nevertheless, studies aimed at exploring the fundamental relationships between concrete's macroscopic mechanical properties and its microstructure under different loading rates and levels are needed if we are to understand, identify, and respond to the basic mechanisms of failure of cement mortars and concrete under dynamic loading conditions.

The present research program, a collaborative effort of Martin Marietta Laboratories and the University of Maryland, attempts to address the above problem by starting with a single, but most important, constituent of concrete, namely, the hydrated cement paste. More specifically, we are studying the relationship between the mechanical properties and microstructure of hydrated cement paste subjected to strain rates up to 10^6 s^{-1} and peak pressures up to 500 kbar. Later, we will include the more complex systems of cement mortars and concrete.

During the first part of 1986, work at Martin Marietta Laboratories was focused on establishing the methodology for preparing specimens of hydrated cement to be tested on the split Hopkinson pressure bar (SHPB), and their characterization by a variety of analytical techniques. At the University of Maryland during this time, the SHPB was modified and adapted for tests on hydrated cement samples. It is now properly calibrated and in operation. During the last part of the year, hydrated cement cylinders with different diameters were prepared and characterized, tested for stress-strain behavior, and then examined for possible microstructural changes. Details of this work are described in the following sections.

II. SAMPLE PREPARATION AND CHARACTERIZATION

Two types of portland cements, Types III and IV, were selected for this study. These two types represent the extremes in phase composition, and are expected to provide a wide range of variations in mechanical properties and microstructural characteristics. Our initial experiments were done using a Martin Marietta Type III portland cement. The chemical and phase compositions of the cement are given in Table 1. Type IV portland cement is not readily available commercially. It has been almost totally replaced by the more economical blended cements (flyash and slag-cements). However, we obtained a limited quantity of Type IV cement (LTS series) from the Portland Cement Association, which will be used in the next phase of our work.

TABLE 1

Chemical and Phase Composition of Type III Cement

Oxide	Amount (%)
Na_2O	<0.2
MgO	2.88
Al_2O_3	4.70
SiO_2	20.09
P_2O_5	0.11
SO_3	4.58
K_2O	0.61
CaO	62.71
TiO_2	0.20
Cr_2O_3	<0.01
Mn_2O_3	0.03
Fe_2O_3	2.48
SrO	0.11
LOI	1.44
C_3S	55.4
C_2S	17.4
C_3A	8.4
C_4AF	7.6

Hydrated cement specimens with different water-to-cement ratios were prepared to obtain a range of microstructures in the paste. The porosity of the hydrated cement paste is directly related to its water/cement ratio, and is found to increase as this ratio increases. The actual water/cement ratios used were 0.25, 0.33, and 0.40. The 0.25 water/cement pastes contained 1% calcium lignosulfonate (by weight of cement) as a water reducer. Mixing preparatory to testing on the SHPB was carried out in accordance with ASTM guidelines.(2)

An appropriate amount of cement was weighed and added to the bowl of a Hobart mixer, as was the amount of distilled water needed for the proper water/cement ratio. The water reducer, when used, was dispersed in the water before it was added to the bowl. The water was allowed to soak into the cement for 15 seconds and the paste was then mixed at low speed (60 rpm) for 2 minutes with a 1-minute interruption for cleaning and removing cement from the paddle and sides of the bowl. After mixing, the cement paste was immediately cast into clean 6 x 6 x 2 in. plexiglass molds and vibrated at medium-to-high intensity on a vibrating table (Sytron) for 10 minutes. The mold was wrapped in plastic wrap and allowed to set for about 24 hours. It was then immersed in a bath containing saturated limewater and cured for 28 days at room temperature.

A week before the end of the 28-day curing period, the set cement paste was demolded and cylindrical specimens, 0.25, 0.375, 0.50, and 0.75 in. in diameter, were cored using precision diamond core drills (Starlite Industries) in a 0.5-in. chuck drill press. A diamond blade saw was used to cut the cores into cylinders having a length/diameter ratio of 1.5. The ends of the cylinders were laped perpendicular and parallel using a machinist's V-block. Figure 1 shows the cored specimens prepared for SHPB testing. Care was taken not to let the cement paste dry during specimen preparation so as to avoid drying shrinkage and subsequent cracking. The cored specimens were stored in limewater until testing.

Portions of the specimens tested on the SHPB were characterized for degree of hydration, porosity, and morphological changes in the hydrated paste. The degree of hydration was estimated as the chemically bound nonevaporable water in the cement paste, as indicated by weight loss upon

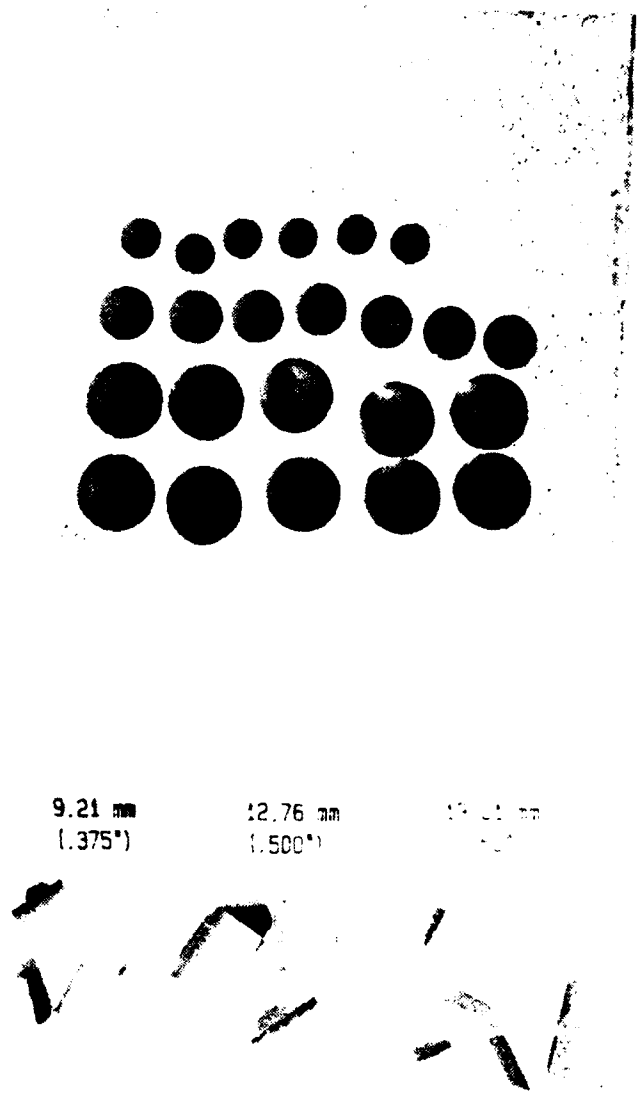

Figure 1. Core specimens of hydrated cement paste for SHPB testing.

heating. For this determination, the paste was ground, washed several times with acetone, oven-dried at 105°C for about 24 hours, and then ignited at 1000°C for 1 hour. The resulting weight loss was taken as a measure of the degree of hydration of the cement.

Scanning electron microscopy (SEM) was used to examine the microstructural development and changes in the cement paste before and after the SHPB tests. A JEOL Model JSM 35-CF scanning electron microscope was used. Additional information on the nature of hydration products was obtained by X-ray diffraction (XRD) and differential thermal analysis (DTA). Use of transmission electron microscopy is also being explored; however, this technique is still not satisfactorily established because the hydrated paste is relatively soft, porous, and very brittle, so that it is difficult to use ion-beam thinning to prepare specimens for examination.

Mercury intrusion porosimetry was used to estimate the porosity of the specimens. The technique involves forcing mercury into the pore system of the paste under external pressure. The pressure required is inversely proportional to the pore radius. This technique provides better information on the capillary pores of the system than other techniques -- an important feature since the capillary porosity of the cement paste is inversely related to its compressive strength.(3) Measurements were made on oven-dried (105°C, 6 hr) pieces of hydrated paste with a Micrometrics Model 9300 Pore Sizer at a contact angle of 117°.(4)

Voids or macropores (larger than 0.1 mm in diameter), which are unavoidably introduced into the cement paste due to entrapped air during mixing, are considered to be the major flaw in the system leading to failure under impact or pressure. In our study, they were determined by the linear intercept method on randomly selected areas of sliced cross sections of the hardened paste (Fig. 2).

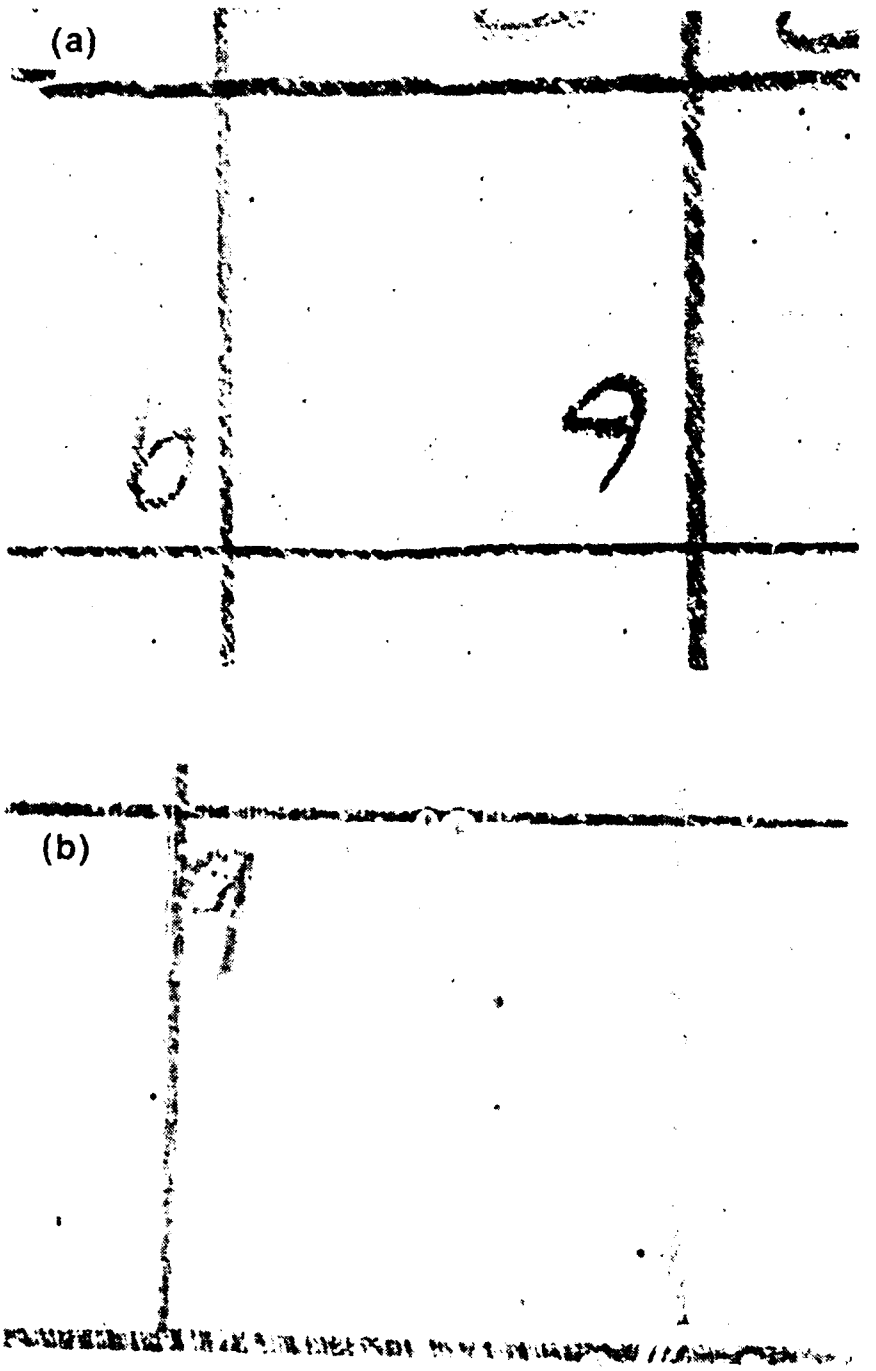

Figure 2. Sliced cross sections from hydrated cement pastes (a) 0.25 water/cement ratio and (b) 0.33 water/cement ratio for air void fraction determination.

III. TESTING METHODOLOGY

The specimens were tested at rates from essentially static to 10^3 s^{-1} on a servo-hydraulically controlled MTS testing machine and a split Hopkinson pressure bar (SHPB). The SHPB operation is based on the one-dimensional elastic wave propagation theory in cylindrical bars.(5) A typical SHPB set-up, shown in Fig. 3, consists of two long bars, commonly referred to as the incident and the transmitter bars, with the specimen located between the bars. The specimen is loaded by a compressive wave of uniform intensity which travels along the incident bar into the specimen. The wave is generated by impacting the end of the incident bar with a projectile bar of the same material and diameter, which is launched from the tube of an air gun.

From one-dimensional wave mechanics, the stress and strain in the specimen, δ_S and ε_S, can be calculated at any point in time from the transmitted elastic strain wave in the transmitter bar, ε_t, and the reflected strain wave in the incident bar, ε_r, as:

$$\delta_S = E\ A\ \varepsilon_t / A_S$$

and

$$\varepsilon_S = 2\ c_0 / L_S \int_0^t \varepsilon_r dt$$

where A and A_S are the cross-sectional areas of the bar and the specimen respectively, L_S is the specimen length, E is the Young's modulus of the bar material, and c_0 is the elastic bar-wave propagation velocity. The average strain rate, $\dot{\varepsilon}_S$, can be calculated as

$$\dot{\varepsilon}_S = -2\ c_0\ \varepsilon_r / L_S.$$

Thus, from one experiment, it is possible to generate a complete dynamic stress-strain plot of the sample material at a given strain rate. If the incident bar and the transmitter bar are made from high yield-strength material, peak loads of 150,000 psi or 10 kbar are easily reached. Typical strain rates for SHPB experiments are on the order of 10^2 to 10^3 s^{-1}.

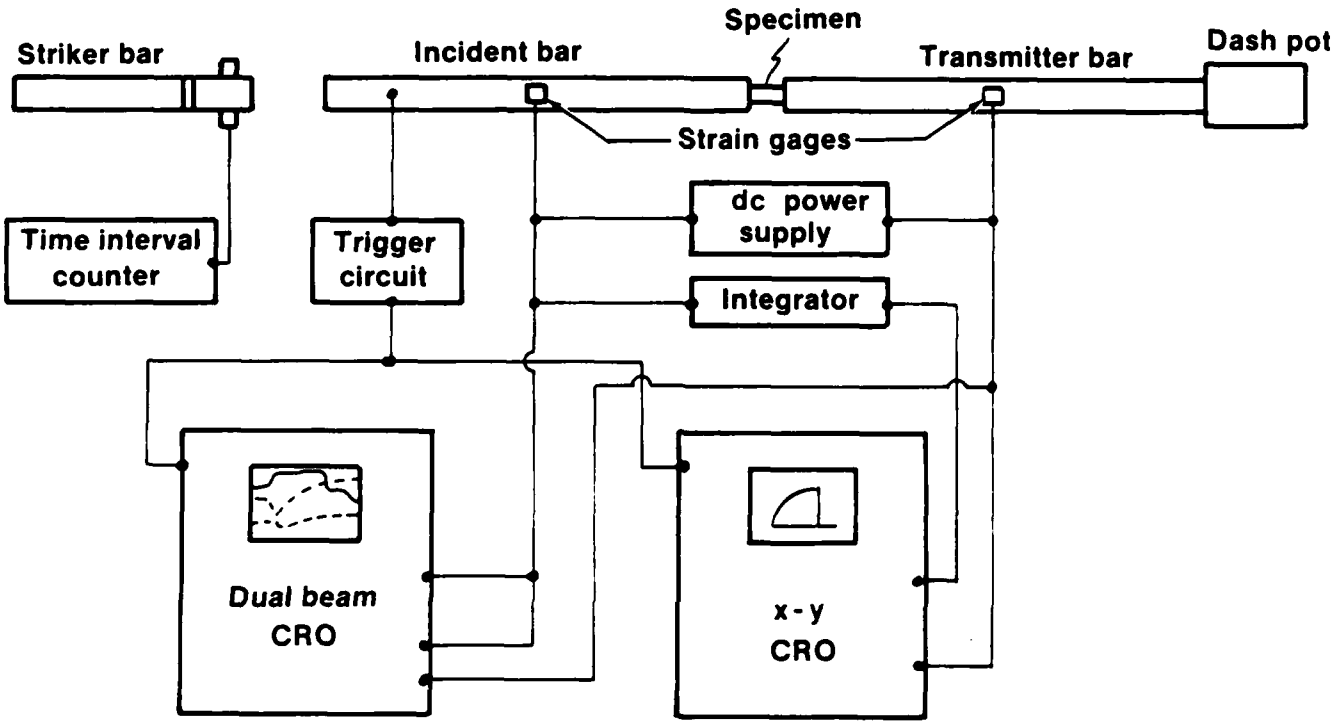

Figure 3. Schematic diagram of SHPB set-up.

The SHPB at the University of Maryland was originally set up for testing very high yield-strength materials. Therefore, for use with cement paste samples, a series of new pressure bars -- 1 in., 3/4 in., and 9/16 in. (25.4 mm, 19 mm, and 14.3 mm) in diameter -- were instrumented with special, high-resistance strain gages. The individual bars are about 6 feet long and matching diameter projectiles have been constructed in varying lengths from about 5 inches (127 mm). With this range of bar diameters, projectile lengths, and varying gas pressures on the launching gun, we can control somewhat the strain rates to which the cement paste samples are subjected. For example, launching a 10-in.-long (254 mm) projectile at 600 in./s (15.2 m/s) into the 3/4-in.-diameter (19 mm) bar with a 0.6-in.-diameter (15.2 mm) cement paste sample between the pressure bars subjects a sample to a strain rate of about 200 s^{-1}. Higher strain rates are accomplished by increasing the projectile velocity and also by increasing the mismatch between sample and pressure bar diameters.

Dynamic instrumentation for the pressure bar apparatus is provided through a Nicolet 2090 digital oscilloscope. Strain output from the strain gages on the incident and transmitter pressure bars is amplified with two BAM-1B dynamic bridge amplifiers and input to the digital oscilloscope. The amplifiers have a 200-kHz frequency response and the Nicolet oscilloscope digitizes at 0.5 μs/point. Data from the Nicolet are transferred to a personal computer for analysis or to various other computers. A hardcopy pen plotting capability is available on the personal computer.

A typical output from the strain gages mounted on the incident and transmitter bars is shown in Fig. 4. In the output from the incident bar (the bold trace), the first pulse is the incident pulse coming from the impact between the projectile and the end of the bar. It is shown as positive, according to compression testing convention. The next pulse, which is due to reflection from the interface with the sample, is tension. Simultaneously, the transmitter bar gages pick up the transmitted compression pulse that has passed through the sample. As explained earlier, the transmitted and the reflected pulses are used for data analysis.

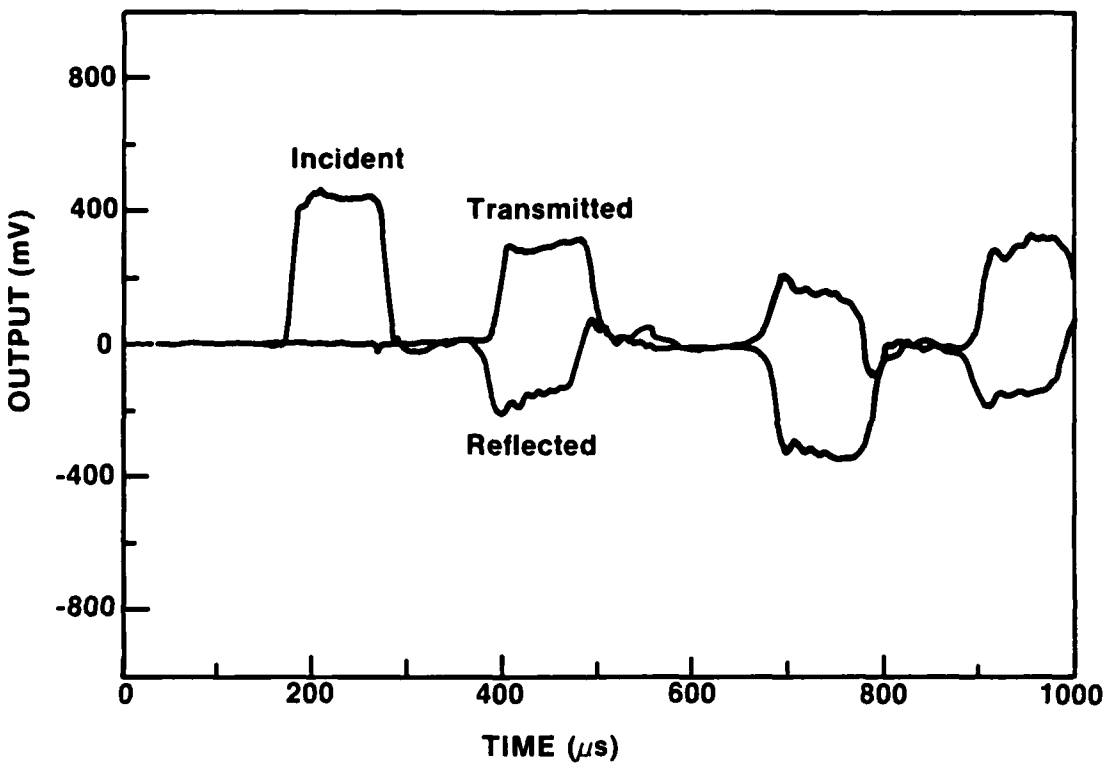

Figure 4. Typical strain-time history plot showing incident, reflected and transmitted pulses.

The calibration and accuracy of the new SHPB arrangement was confirmed by a series of tests on 6061-T6 aluminum, an aluminum alloy that is insensitive to strain rates up to about 1000 s^{-1}. Various sample diameters were tested so as to achieve a range of strain rates from 374 to 3290 s^{-1}. The dynamic stress-strain results gave similar curves, with a dynamic yield strength very close to the static value of 48 ksi. Figure 5 shows the results for three of the lower strain-rate tests.

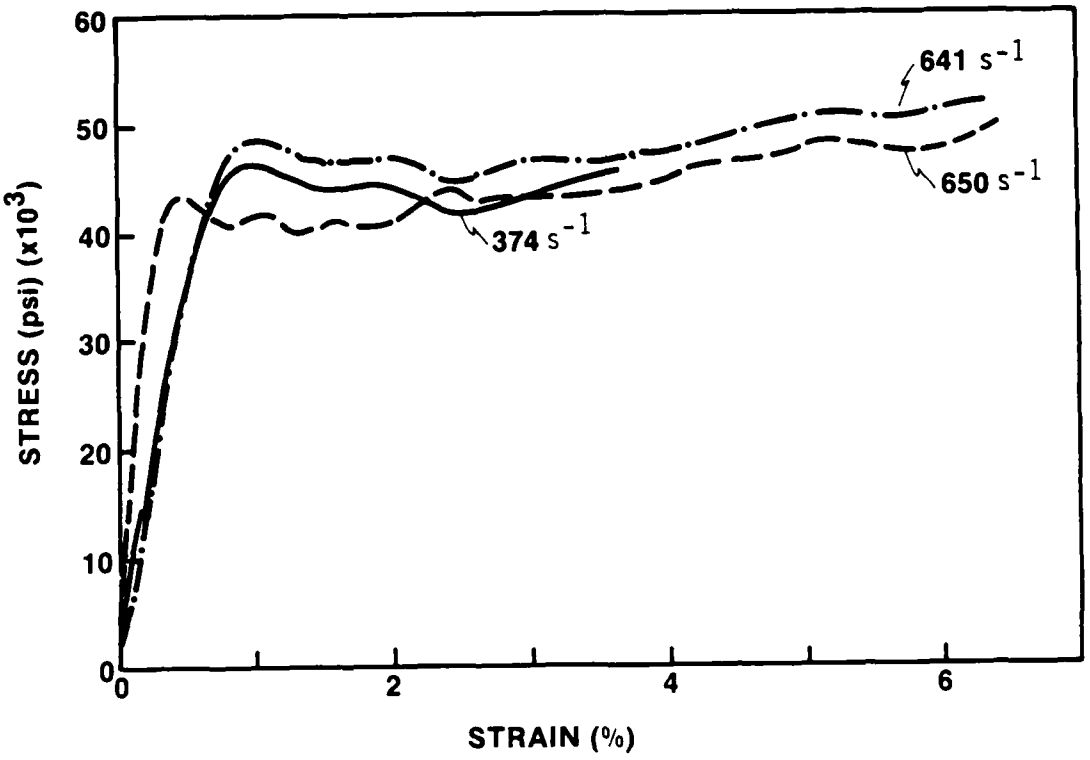

Figure 5. Stress-strain curves for 6061-T6 aluminum.

IV. RESULTS AND DISCUSSION

Figures 6 and 7 show the plots of stress-strain data obtained on the MTS machine and the SHPB, respectively. Two distinct trends in the stress-strain behavior of cement paste over the range of strain rates are immediately noticeable. At low strain rates (all MTS data and SHPB data up to about 250 s^{-1}), the ultimate stress increases roughly linearly with an increase in the strain rate. At higher strain rates (SHPB data above 250 s^{-1}), the ultimate stress appears to reach, more or less, a plateau, although there is wide scatter in the data. While the presence of two distinct trends suggests that different mechanisms may be operating at low and high strain rates, it is too early to speculate on the reasons for the observed behavior. The specimens were found to fragment into a greater number of pieces at high strain rates.

The stress data also show a dependence on the water/cement ratio of the hydrated cement paste, with the ultimate stress highest for specimens with a water/cement ratio of 0.25. Specimens with a water/cement ratio of 0.40 showed the lowest stress value, although not significantly lower than those with a water/cement ratio of 0.33.

The above observations appear to correlate, at least qualitatively, with the porosity of the hydrated systems. The hydration rate, and hence the porosity, of the cement paste is directly related to its water/cement ratio. The porosity of the cement paste is due to its hydration products, especially the calcium silicate hydrates (C-S-H), the highly porous, semi-amorphous material that constitutes about 70-75% of the hydrated material in the paste. At any given time, the degree of hydration, and hence the amount of hydration products, is lower for cement paste with a lower water/cement ratio. Table 2 gives data on the degree of hydration (estimated as bound water), porosity, and air-void fraction (macropores with diameter greater than 0.1 mm) of the cement pastes.

TABLE 2

Degree of Hydration and Porosity of Cement Pastes

Water/Cement Ratio	Bound Water (%)	Porosity (%) (<0.1 mm)	Void Fraction (%) (>0.1 mm)
0.25	15.6	15.2	0.68
0.33	16.7	18.3	1.91
0.40	18.0	22.2	1.04

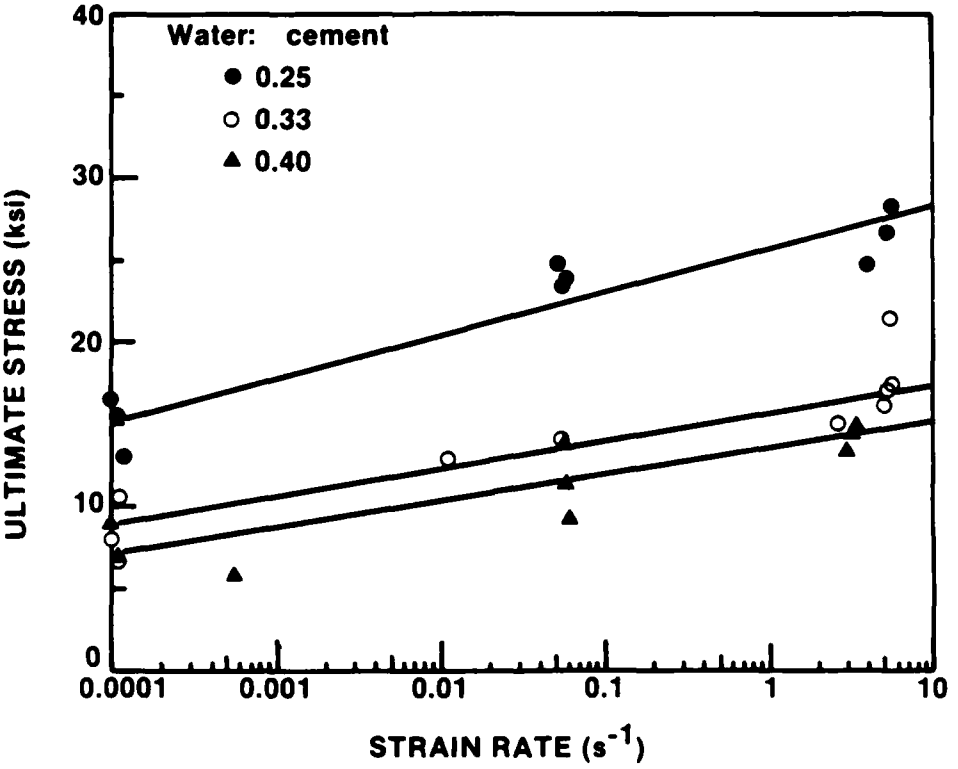

Figure 6. MTS test results showing ultimate stress versus strain rate at maximum stress for hydrated cement pastes (28 days).

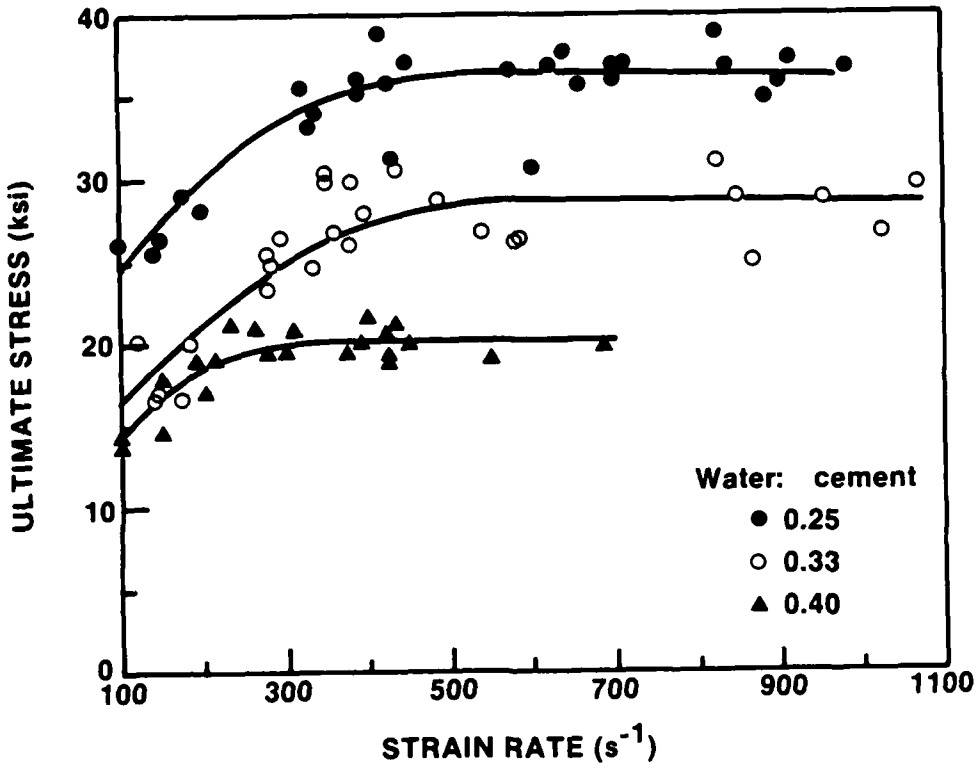

Figure 7. SHPB test results showing ultimate stress versus strain rate at maximum stress for hydrated cement pastes (28 days).

Both the degree of hydration and porosity are low for the paste with the 0.25 water/cement ratio as compared with other pastes. Figure 8 is a plot of mercury porosimetry data showing the pore size distribution of the three pastes. The paste with the 0.25 water/cement ratio is also seen to contain a larger proportion of smaller sized capillary (<<0.1 mm in diameter) pores than the other two pastes. As expected from the general porosity-strength relationship of brittle materials, this paste shows the highest ultimate strength. Furthermore, pastes with a low degree of hydration contain a substantial amount of unhydrated cement particles. These hard "aggregates" can also be a factor in the increased strengths of such pastes under compression.

For the other two pastes (0.33 and 0.40 water/cement ratios) also, the stress behavior shows an inverse relationship with total porosity in the expected order, even though the proportion of pores in the larger capillary pore region (Fig. 8) and the macropore (air void) content (Table 2) for the 0.33 ratio paste are larger than those for the 0.40 ratio paste. These discrepancies in the distribution of larger capillary pores and air voids are presumably due to unavoidable experimental inconsistencies during sample preparation. Nevertheless, they serve to emphasize the effect of porosity on the mechanical properties of hydrated cement.

The specimens were examined by SEM before and after the SHPB tests to determine the microstructure of the fracture surface and any possible morphological changes as a result of loading. Additional examinations were conducted by XRD and DTA. The latter two techniques did not, or were unable to, reveal any changes in the nature and crystallinity of hydration products. SEM examination, however, showed that the fracture surface of the specimens consisted predominantly of the calcium silicate hydrate (C-S-H) phase (Fig. 9). This was observed at all water/cement ratios. Very little $Ca(OH)_2$ was found on the fracture surface. The cracks on the fracture surface showed a rather complex pattern.

In a fully hydrated cement paste, $Ca(OH)_2$ would constitute about 20-25% of the hydration products. For our pastes, with approximately 70-80% degree of hydration, we had expected at least 10-15% of the fracture surface to consist of $Ca(OH)_2$ if the microstructure was irrelevant in determining the fracture behavior. Some previous studies on crack propagation in cement pastes under static loading have indicated that in the

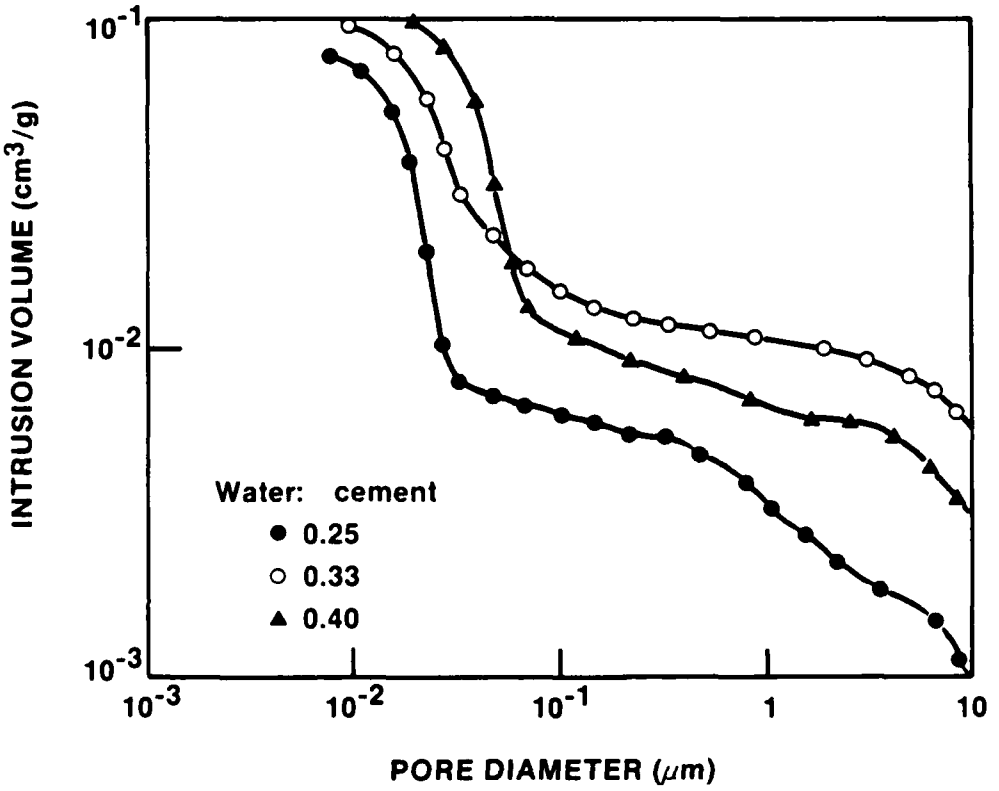

Figure 8. Pore size distribution in hydrated cement pastes.

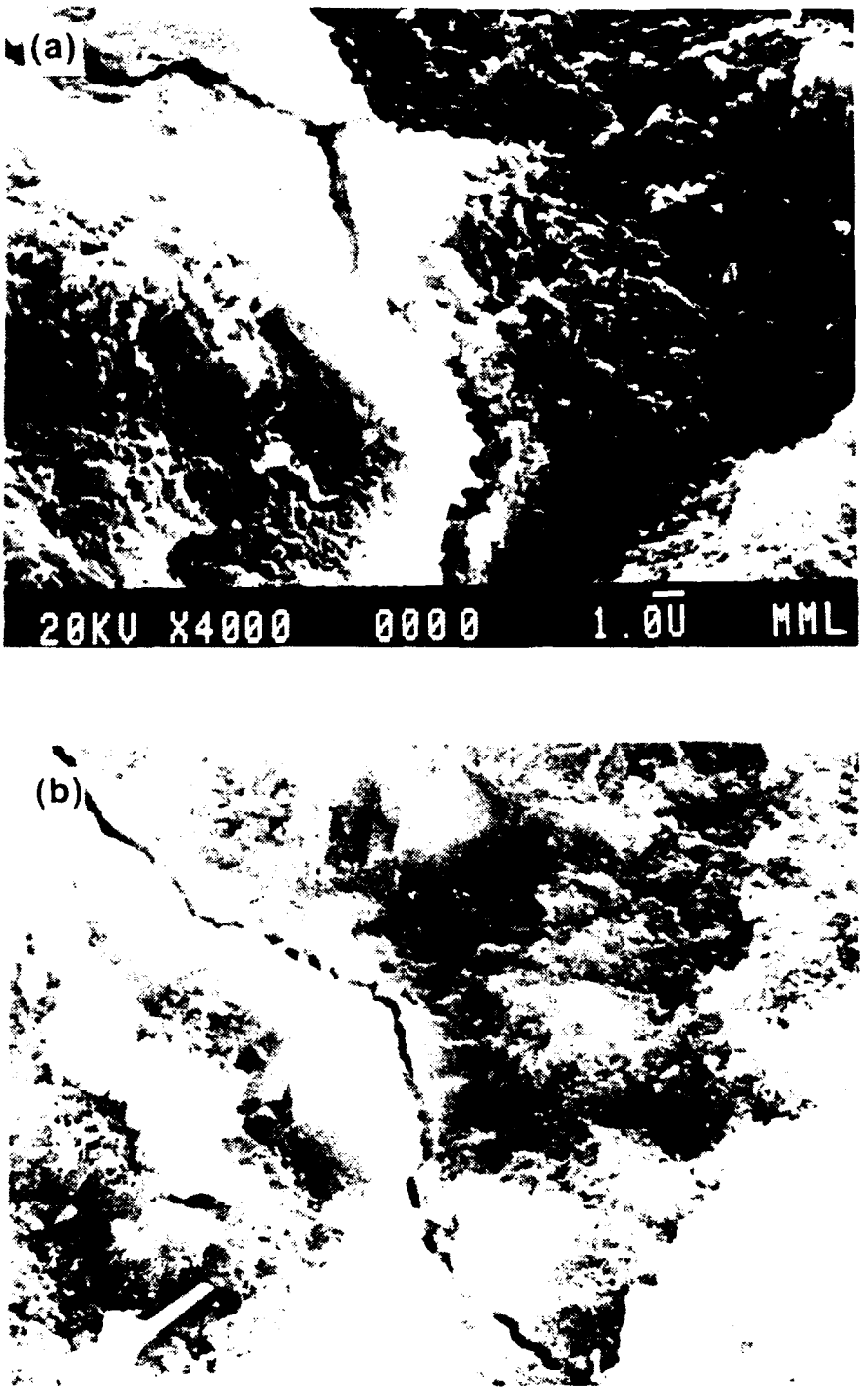

Figure 9. Scanning electron micrographs showing fracture surface of hydrated cement paste (w/c - 0.33) under dynamic compression. The fracture surface consists mostly of the C-S-H phase.

early stages of hydration, C-S-H is the softer phase in the paste and, therefore, the more likely region to fracture; later, as the paste matures, the strengths of C-S-H and $Ca(OH)_2$ probably become similar so that there is no particular region in which cracks preferentially propagate.[6-8] Our data suggest that even after 28 days, and in a relatively mature paste, fracture preferentially occurs through the more porous C-S-H. This behavior was observed at both low and high rates of loading. The specimens did show fracture through $Ca(OH)_2$, usually parallel to the basal planes (Fig. 10a), but occasionally across it (Fig. 10b). The latter mode of fracture was found to be more common at higher strain rates. In some instances, cracks on the fracture surface were also seen between the hydrated and unhydrated cement particles (Fig. 11).

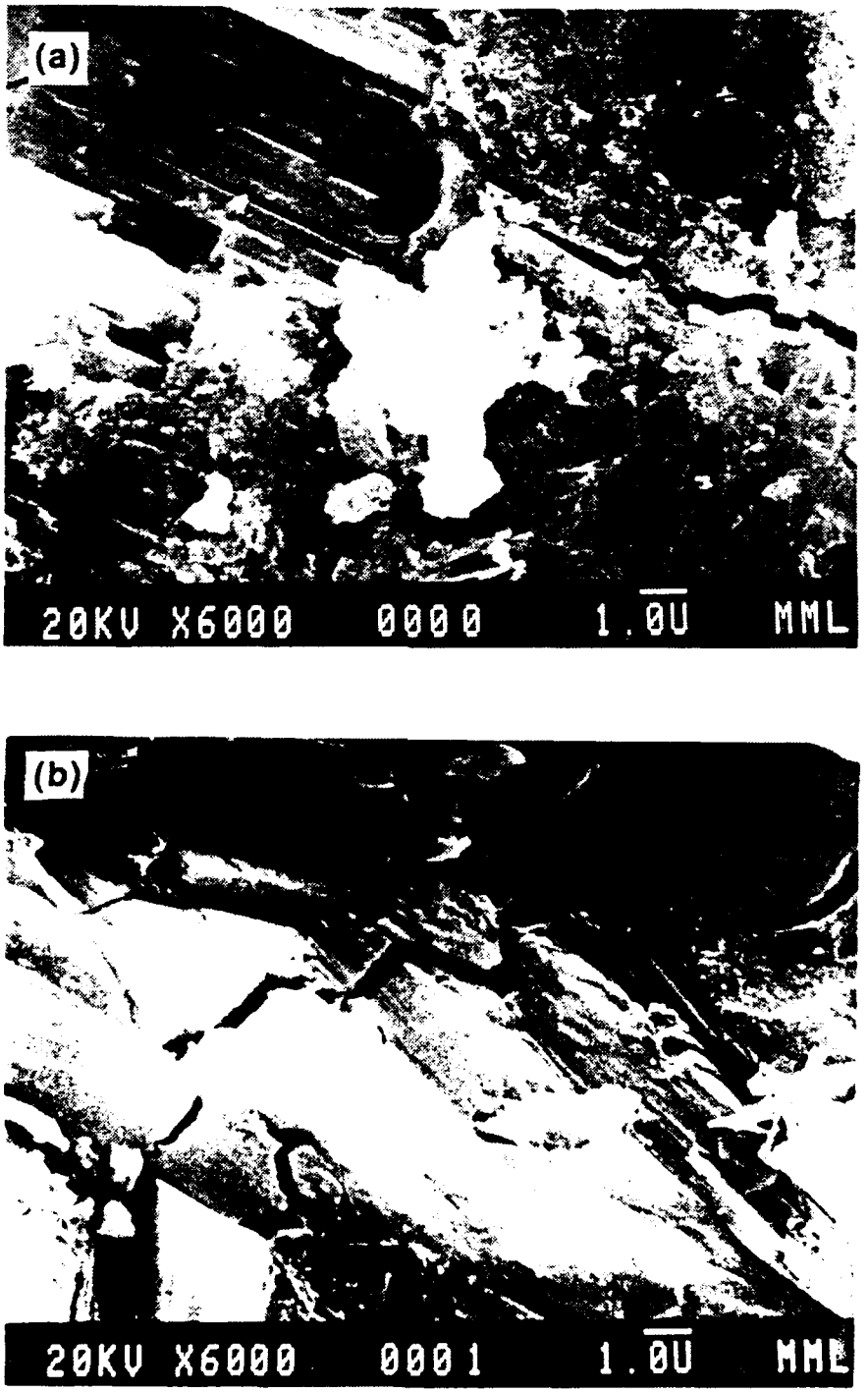

Figure 10. Scanning electron micrographs showing fracture in the $Ca(OH)_2$ phase of the hydrated cement paste (w/c = 0.40): (a) through basal plane and (b) across the basal plane.

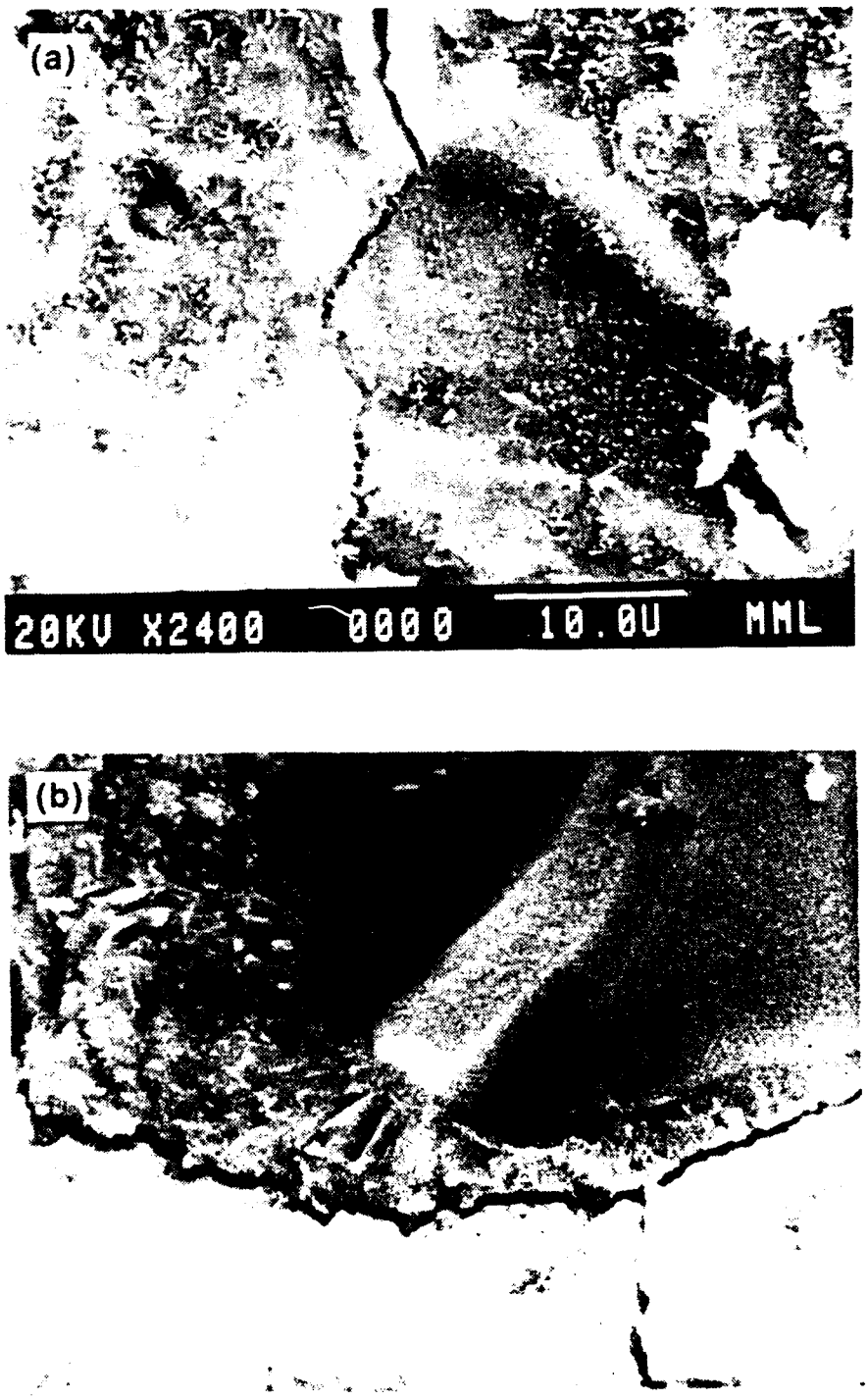

Figure 11. Scanning electron micrographs showing cracks between hydrated and unhydrated cement particles on the fracture surface of hydrated cement paste (w/c = 0.25).

V. CONCLUSIONS

Our initial investigations using a Type III portland cement have shown two distinct trends in the stress-strain behavior of cement pastes. At low strain rates (<250 s^{-1}), the ultimate stress increases more or less linearly, whereas at higher rates (>250 s^{-1}), it appears to reach a somewhat limiting value over the range of strain rates used.

While it is too early to speculate on the reasons for the observed stress-strain behavior, our initial results suggest that porosity of the hydrated cement paste is a dominating factor in determining the strain-rate response. Fractures and cracks appear to go through the C-S-H phase of the hydrated paste even at relatively mature age. Additional data are needed on individual clinker minerals and cements with different mineralogical compositions over a wide range of strain rates if we are to understand and explain the observed stress-strain behavior of hardened cement paste.

VI. FUTURE PLANS

In the coming months, we will continue to work on the stress-strain behavior of cement pastes made with additional cements of different mineralogical compositions. As mentioned earlier, a Type IV portland cement has been obtained from the Portland Cement Association. This cement represents the other extreme in mineralogical composition from Type III, and should give additional information on the effect of the hydration process on the behavior of cement paste under loading.

Furthermore, in view of the complexity of the microstructure of the hydrated cement paste, we have decided to include in our tests pastes made from pure cement minerals, C_3S, C_2S, and C_3A. The behavior of pure minerals, and their characterization, will help us to isolate and better understand the effect of high strain rate on the microstructure of complex cement systems. For example, pastes of C_3S and C_2S might confirm or modify the conclusions of the present study on the mode of fracture under stress, and also help to ascertain the effects, if any, of high strain rate on the morphology of $Ca(OH)_2$ and C-S-H. TEM measurements on such samples will also be less ambiguous.

The range of strain rates will be further extended. The paste will be subjected to strain rates at least an order of magnitude greater than those presently used. We will also conduct tests on specimens hydrated for extended periods of time, such as 90 and 180 days.

All modifications in the SHPB set-up at the University of Maryland, mentioned in the previous report, have been made and checked. The modified SHPB is capable of quantifying more accurately the sample response under stress. It is now properly calibrated and fully operational.

VII. REFERENCES

1. S. Mindess and S.P. Shah (Eds.), "Cement-Based Composites: Strain Rate Effects on Fracture," Proc. Mater. Res. Soc. Symp., Vol. 64, Mat. Res. Soc., Pittsburg, PA (1986).

2. ASTM, 1978 Annual Book of Standards, Part 13, Philadelphia, PA (1978).

3. G.J. Verbeck and R.A. Helmath, Proc. 5th Int. Symp. Chemistry of Cement, Vol. 3, Tokyo, pp. 1-32 (1968).

4. D.N. Winslow and S. Diamond, J. Mater., 5, 564 (1970).

5. J.A. Zukas, T. Nicholas, H.F. Swift, L.B. Greszczuk and D.R. Curran, "Impact Dynamics," Chapt. 8, p. 277, J. Wiley & Sons, New York (1982).

6. R.L. Berger, Science, 175, 626 (1972).

7. R.L. Berger, F.V. Lawrence, Jr. and J.F. Young, Cem. Concr. Res., 3, 497 (1973).

8. B. Marchese, Cem. Concr. Res., 7, 9 (1977).

9. S. Mindess, in Proc. Eng. Sci. Found. Conf. 1979, Rindge, NH, p. 175, Eng. Foundation, New York (1980).

END

5-87

DTIC